KFUPM
Journal of Undergraduate Research International

Diamond Open Access 25

Article Chemical Engineering

Effect of Electrodeposition Strategy on Ni–Co Catalysts for Electrochemical HMF Oxidation to FDCA

Joud Aljohani and Wasif Farooq*

Cite https://doi.org/10.64589/juri/231538

Submitted: April 24, 2026 **Revised:** May 15, 2026 **Accepted:** May 18, 2026

ABSTRACT

The conversion of biomass-derived molecules into sustainable raw materials for bioplastics has attracted significant attention, particularly for the oxidation of 5-hydroxymethylfurfural (HMF) to 2,5-furandicarboxylic acid (FDCA). In this study, Ni–Co bimetallic catalysts were synthesized via three electrodeposition strategies: stepwise (Ni-first and Co-first), mixed, and pulse deposition. The influence of the deposition strategy on morphology, composition, and electrochemical performance was investigated. Scanning electron microscopy revealed distinct morphologies, with the pulse-deposited sample exhibiting a highly uniform and densely packed nanostructure. Energy-dispersive X-ray spectroscopy confirmed that the catalyst composition was governed by the deposition method. Variations in these properties influenced electrocatalytic performance during HMF oxidation reaction (HMFOR) and the oxygen evolution reaction (OER). The pulse-deposited sample exhibited superior overall performance, achieving current densities of 187 and 165.8 mA cm^{-2} for HMFOR and OER, respectively, at 1.72 V vs. RHE. A comparison based on the required potential showed that the pulse-deposited catalyst exhibits a lower onset potential (~1.33 V vs. RHE) and required lower potentials to reach 10 and 25 mA cm^{-2}, indicating improved energy efficiency. It also demonstrated the lowest Tafel slope (98.9 mV dec^{-1}) and smallest charge-transfer resistance (0.0392 Ω), confirming faster reaction kinetics. Complete HMF conversion was achieved, and the FDCA yield reached 28.52% after 180 min of electrolysis at 1.50 V vs. RHE, indicating that further optimization is required to improve FDCA selectivity. The pulse-deposited Ni–Co catalyst exhibits superior activity, enhanced kinetics, and reduced energy requirements, rendering it a promising catalyst for efficient electrochemical HMF oxidation.

Keywords: 5-hydroxymethylfurfural (HMF), 2,5-furandicarboxylic acid (FDCA), Ni–Co bimetallic catalysts, electrodeposition, electrocatalytic oxidation, biomass valorization

1. INTRODUCTION

The electrochemical oxidation of biomass-derived molecules has gained significant attention for the production of value-added chemicals in a more sustainable manner. Abundant biomass, particularly lignocellulosic materials from agricultural residues and plant-based sources, can be used as a renewable source of oxygenated platform molecules[1]. A key platform molecule is 5-hydroxymethylfurfural (HMF), which is commonly obtained by the dehydration of sugars such as glucose and fructose. Since HMF contains both aldehyde and alcohol groups, it can be converted into a range of useful products[2], such as 2,5-furandicarboxylic acid (FDCA). Notably, FDCA is considered a bio-based alternative to terephthalic acid and can be used in polymer production[2]. Compared with conventional thermochemical oxidation, electrochemical oxidation proceeds under milder conditions without the requirement for strong oxidants. It also provides superior control over product selectivity depending on the catalyst[2]. However, HMF oxidation involves multiple steps, including both alcohol and aldehyde oxidation, resulting in relatively slow reaction kinetics[3,4].

Ni-based catalysts have been widely investigated as efficient anodic materials for the electro-oxidation of biomass-derived molecules such as HMF[5]. In alkaline media, Ni-based catalysts typically operate at potentials of ~1.3–1.5 V vs. the reversible hydrogen electrode (RHE), where the in situ formation of NiOOH as the active phase drives the oxidation process[4,6]. Nevertheless, Ni-based systems often suffer from relatively high onset potentials and slow reaction kinetics, which limit their overall efficiency for HMF electro-oxidation[4].

To overcome these limitations, bimetallic systems, particularly Ni–Co-based catalysts, have been extensively explored. Compared to monometallic Ni catalysts, Ni–Co systems exhibit enhanced catalytic performance owing to the synergistic interactions between the Ni and Co sites. For instance, Ni–Co layered hydroxide catalysts can achieve a low onset potential of ~1.20 V vs. RHE and deliver high FDCA yields of up to ~95.6% with Faradaic efficiencies (FE) of ~90.5%[4]. Furthermore, heterogeneous $NiCo(OH)_2/NiCo_2O_4$ catalysts have been shown to operate at ~1.317 V, achieving 20 mA cm^2, while maintaining a high FDCA selectivity (86.7%) and FE of 93.1%[7].

Published under an exclusive license by KFUPM

In addition to superior activity, Ni–Co catalysts also demonstrate faster reaction kinetics. For example, the incorporation of Co can reduce the Tafel slope from ~36.7 to ~27.6 mV dec^{-1}, indicating enhanced charge-transfer properties [7]. These improvements are generally attributed to the synergistic effect between Ni and Co, where Ni facilitates oxidation while Co promotes the transformation of reaction intermediates [4]. Although Ni–Co systems exhibit clear advantages over Ni catalysts, their performance strongly depends on catalyst structure, composition, and electrocatalytic behavior, highlighting the requirement for further optimization to achieve efficient and stable HMF electro-oxidation systems.

Electrodeposition is widely employed for catalyst preparation owing to its simplicity and ability to provide precise control over catalyst composition and morphology. Compared with other techniques, this method offers superior uniformity and direct growth on conductive substrates, thereby enhancing electrical connectivity. However, it often suffers from limited control over crystallinity and demands careful adjustment of the deposition parameters [8]. Despite the promising performance of Ni–Co catalysts, the influence of different electrodeposition strategies on their structure–performance relationship remains insufficiently understood.

In this study, Ni–Co catalysts are prepared using different electrodeposition methods, including stepwise (Ni-first and Co-first), mixed, and pulse deposition. The influence of the deposition strategy on the catalyst morphology, composition, reaction kinetics, and electrocatalytic performance in the HMF oxidation reaction (HMFOR) and the oxygen evolution reaction (OER) is systematically investigated.

2. METHODOLOGY

2.1. Materials. Cobaltous nitrate hexahydrate (99.0%) was obtained from Analar, Poole, UK. Nickel(II) nitrate hexahydrate (97%), potassium hydroxide (KOH, 85%), and HMF (99%) were purchased from Sigma-Aldrich, St. Louis, MO, USA. All chemicals were used as received without further purification. Deionized water was used to prepare all solutions. Commercial Ni foam (NF) with a thickness of 2 mm and pore density of 75 PPI was used as the conductive substrate for catalyst deposition. Prior to electrodeposition, the NF (1 ×1 cm^2) was cleaned to remove surface impurities and surface oxides. Specifically, the foam was initially ultrasonicated in a 1 M HCl solution at 30 °C for 30 min to remove any surface oxides, followed by similar treatment in ethanol to eliminate organic contaminants. The cleaned samples were rinsed with deionized water and dried in an oven at 60 °C for 24 h. The HMF conversion and FDCA yield were analyzed using a Shimadzu HPLC system equipped with a C18 Shim Pack Velox column (2.7 µm, 50 ×2.1 mm). The mobile phase consisted of 5 mM ammonium formate and methanol at a flow rate of 0.1 mL min^{-1}.

2.2. Experimental.

2.2.1. Synthesis of the Ni–Co catalysts. The electrolyte for Ni–Co electrodeposition was prepared from cobalt(II) nitrate and nickel(II) nitrate hexahydrate solutions (0.5 M each) based on the optimized Ni/Co molar ratio of 4:1, and electrodeposition was performed using a standard three-electrode system. Stepwise electrodeposition was performed with Co deposition at −1.5 V, followed immediately by Ni deposition under the same conditions (Co-first sequence). The deposition time was 200 s for the mixed Ni–Co catalyst and for each step in the stepwise deposition process. Pulse deposition was performed for 150 cycles, corresponding to a total deposition time of 600 s.

In the corresponding Ni-first sequence, the order of deposition was reversed, with deposition performed under identical conditions. For the mixed deposition protocol, Ni and Co precursor solutions (0.5 M each) were combined according to a Ni/Co molar ratio of 4:1, and electrodeposition was performed at −1.5 V for 200 s. For pulse deposition, an initial pulse of −0.5 V was applied for 1 s, followed by −1.5 V for 2 s, and −0.5 V for 1 s. Deposition was conducted over 150 cycles with an off potential of 0 V. The morphology and composition of the prepared Ni–Co catalysts were examined using FE-SEM (Thermo Scientific Quattro S, 10 kV) coupled with EDX (INCA Energy 200, Oxford Instruments, UK). TEM analysis was performed using a JEOL JEM-2100F operated at 300 kV. The mass loadings of the prepared catalysts are presented in Table S1, revealing that pulse deposition resulted in the highest mass loading, followed by the Co-first approach, mixed deposition, and finally, the Ni-first sequence. A similar trend was observed for the estimated thickness values, indicating a direct correlation between mass loading and film thickness. These trends were attributed to differences in the deposition kinetics and metal reduction behavior, implying that Co deposition promotes subsequent Ni growth, possibly by providing a more favorable nucleation surface. The thickness (T) of each electrodeposited Ni–Co layer was estimated using a density-based gravimetric method, as expressed in Equation S1.

2.2.2. Electrochemical Measurements. A standard three-electrode system in the single-cell configuration was employed to perform the electrochemical measurements. Electrodeposition was performed using a CorrTest CS310M electrochemical workstation (Wuhan CorrTest Instruments, China) with Ag/AgCl as the RE, Pt as the CE, and NF as the WE. Electrochemical analyses of the OER and HMFOR were carried out in an H-cell using a Gamry potentiostat (Interface 1010E) with Hg/HgO as the RE, Pt as the CE, and Ni–Co deposited on NF as the WE. Notably, Hg/HgO was employed during electrochemical testing because of its high stability under strong alkaline conditions and high anodic potentials. The measured potentials were converted to the RHE scale using the following equation:

$$E(RHE) = E(Hg/HgO) + 0.924\ V.$$

The catalytic activity toward the OER and HMFOR was evaluated using LSV at a scan rate of 5 mV s^{-1}. The corresponding Tafel slopes were derived from the LSV curves to evaluate the reaction kinetics. Electrochemical impedance spectroscopy (EIS) was performed to investigate the charge-transfer resistance and interfacial kinetics. Cyclic voltammetry (CV) was conducted in the non-Faradaic region at various scan rates to estimate the double-layer capacitance (C_{dl}), which was subsequently used to evaluate the electrochemically active surface area (ECSA).

The methodology employed in the current study is outlined in Figure S1.

3. RESULTS AND DISCUSSION

3.1. Morphological Characterization. SEM was employed to examine the surface morphologies of the Ni–Co catalysts prepared using the different electrodeposition strategies. Clear morphological differences were observed among the samples, as shown in Figure S3, confirming that the deposition strategy affected the nucleation and growth of the Ni–Co deposits. Specifically, Figure S3a shows an SEM image of the stepwise (Ni-first) sample, which exhibits a smoother surface, suggesting that the initial Ni layer provided a more homogeneous nucleation platform. However, the resulting dense structure may hinder electron transfer. In contrast, the stepwise (Co-first) sample displays a rough and nonuniform surface with localized agglomeration (Figure S3b). This morphology can be attributed to heterogeneous nucleation during the initial Co deposition step and the uneven subsequent growth of Ni. The mixed deposition sample displayed a uniform morphology with closely packed particles, consistent with co-nucleation during simultaneous deposition (Figure S3c). Notably, the pulse-deposited catalyst (Figure S3d) exhibited a highly textured and porous surface with finer features. These observations suggest that the use of an intermittent potential during pulse deposition helps limit particle growth while generating new nucleation sites, resulting in a rougher and more porous surface[4].

Figure S4 presents the EDX spectra and elemental composition of the prepared Ni–Co catalysts, confirming the successful deposition of Ni–Co oxide/hydroxide films. Although all samples exhibited similar elemental distributions, the Ni/Co ratio varied with the deposition strategy, indicating its strong influence on the surface composition. While Ni remained the dominant element, the Ni-first catalyst showed the highest apparent Co incorporation, which can be attributed to the surface-sensitive nature of EDX, where the Co-rich outer layer contributes more strongly to the detected signal[9]. The pulse-deposited sample exhibited a higher Ni content with lower oxygen incorporation, consistent with the formation of a denser deposited layer observed by SEM. In contrast, the mixed and stepwise-deposited samples showed greater variations in the Ni/Co ratio, suggesting a less homogeneous elemental distribution. These compositional differences correlate with the superior HMFOR and OER performances of the pulse-deposited catalyst, indicating that the deposition strategy influences both the surface chemistry and electrocatalytic activity.

The presence of oxygen in all samples further indicates the formation of oxide/hydroxide phases rather than purely metallic species[7,10]. Such surface species have been reported to promote charge transfer and surface redox activity during HMFOR and OER[10]. Similar behavior has been reported for NiCo(OH)2/NiCo2O4 catalysts, where oxide/hydroxide surface species enhanced the electrochemical activity during HMFOR[7].

In the X-ray diffraction (XRD) spectrum of the pulse-deposited Ni–Co catalyst (Figure S5), the diffraction peaks observed at ~44.5°, 51.8°, and 76.4°correspond to the (111), (200), and (220) planes of metallic Ni, respectively, which originate mainly from the NF substrate[11]. The dominance of these reflections indicates that the highly crystalline substrate produces stronger diffraction signals than the deposited catalyst layer.

To further examine the deposited layer, the low-angle region was enlarged (Figure S5, inset), revealing weak and broad diffraction features associated with Ni–Co hydroxide-related phases[11]. These broad reflections indicate that the electrodeposited layer possesses relatively low crystallinity, consistent with previous reports of thin electrodeposited Ni–Co hydroxide films[11]. Although the EDX analysis confirmed the presence of significant amounts of O together with Ni and Co in the deposited layer, no distinct diffraction peaks corresponding to crystalline Co or Co oxides were observed. This can be attributed to the relatively thin deposited layer together with the dominant diffraction contribution from the highly crystalline NF substrate. Similar observations have been reported for weakly crystalline or partially amorphous electrodeposited Ni–Co hydroxide films[11,12]. Furthermore, the oxygen detected by EDX supports the formation of oxygen-containing Ni–Co surface species rather than purely metallic phases, consistent with previous reports of oxide/hydroxide surface species and O–M bonding environments in Ni–Co-based hydroxide systems[12]. The combined EDX and XRD results therefore suggest that the deposited catalyst layer mainly consists of thin and weakly crystalline Ni–Co oxide/hydroxide surface species formed on the NF substrate.

3.2. Electrochemical Analysis. The electrocatalytic performances of the Co-first, Ni-first, mixed, and pulse-deposited catalysts in the OER and HMFOR were subsequently evaluated using LSV. Measurements were performed in 1.0 M KOH with a Hg/HgO RE at a scan rate of 5 mV s^{-1}, as detailed in Figure 1 and Table S2, where clear differences in electrochemical behavior can be observed among the samples. For the Co-first catalyst, the HMFOR onset occurred at a lower potential and the current density exceeded that of the OER over a wide potential range, indicating more favorable HMFOR kinetics. The Ni-first sample followed a similar trend but with lower current densities, indicating reduced electrocatalytic activity. The mixed sample exhibited delayed reaction onset and lower current densities for both reactions, indicating a less favorable overall electrocatalytic performance. Nevertheless, the HMFOR was favored over the OER, consistent with the results obtained for the other catalysts. As shown in Figure 1, the pulse-deposited sample demonstrated superior electrocatalytic performance, exhibiting a higher current density at elevated potentials and relatively stable activity over a wide potential range. This behavior may be due to the more uniform active-site distribution and improved charge-transfer properties generated through pulse deposition. In contrast, the stepwise-deposited samples displayed a more pronounced drop in current density at intermediate potentials, indicating a less stable electrochemical response.

Tafel plots were derived from the LSV curves to evaluate the OER and HMFOR kinetics (Figure 2). The slopes were obtained from the linear region of the plot of η versus log(j), according to Equation S2[13]. For all samples, the Tafel slope for the HMFOR was significantly lower than that for the OER, indicating faster reaction kinetics for HMF oxidation. This behavior is consistent with the less kinetically demanding HMFOR pathway,

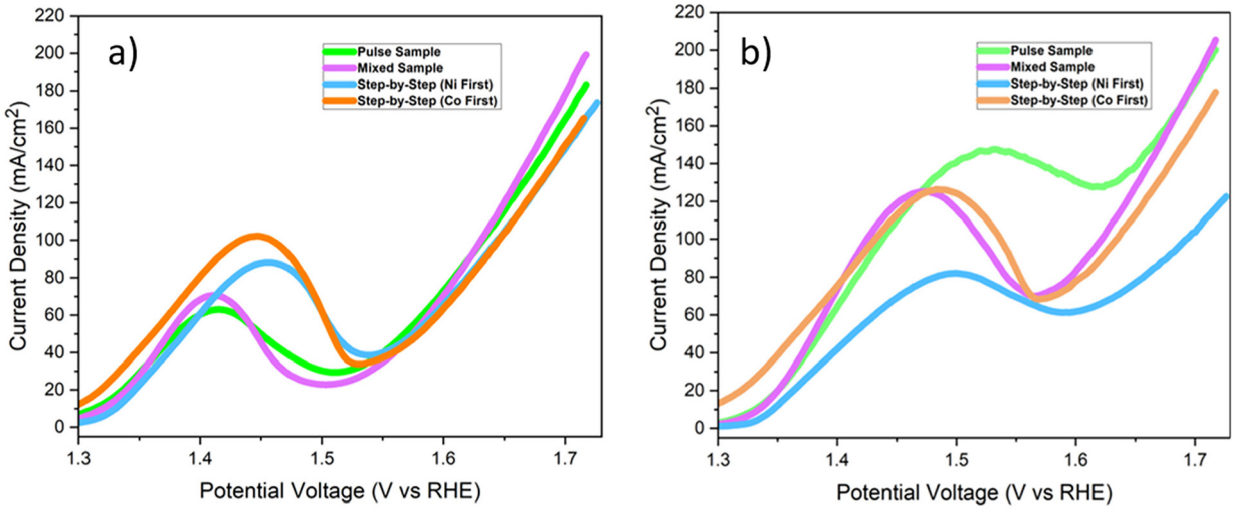

Figure 1. LSV curves of the prepared catalysts toward (a) OER and (b) HMFOR in 1.0 M KOH

which does not involve O–O bond formation[5,13]. Tafel analysis further revealed that the electrocatalytic kinetics strongly depended on the deposition strategy. For the HMFOR, the pulse-deposited catalyst exhibited the lowest Tafel slope (98.9 mV dec^{-1}), indicating the most favorable reaction kinetics. In comparison, the mixed catalyst showed a higher slope of 129.3 mV dec^{-1}, while the Ni-first and Co-first catalysts exhibited larger values of 142.3 and 146.5 mV dec^{-1}, respectively. These results suggest that pulsed deposition promotes a more efficient distribution of active Ni–Co species and facilitates charge transfer during the HMFOR. All samples exhibited considerably higher Tafel slopes for the OER, reflecting the more kinetically demanding multielectron OER process. The mixed catalyst displayed the lowest OER Tafel slope (199.6 mV dec^{-1}), indicating relatively improved OER kinetics compared with the stepwise- and pulse-deposited samples. The Ni-first and Co-first catalysts showed slopes of 230.2 and 256.9 mV dec^{-1}, respectively, while the pulse-deposited sample exhibited the highest value (271.15 mV dec^{-1}). Thus, although pulse deposition significantly enhances HMFOR kinetics, this enhancement was less pronounced for the OER kinetics under the current conditions.

EIS was employed to further elucidate the interfacial charge-transfer behavior and reaction kinetics of the prepared catalysts during the OER and the HMFOR. Measurements were conducted at fixed potentials of ~1.62 and 1.47 V (vs. RHE) for the OER and the HMFOR, respectively. The Nyquist plots obtained under the corresponding reaction conditions are shown in Figure 3a,c, and the equivalent circuit models used to fit the experimental data are shown in Figure 3b,d.

3.2.1. EIS data fitting. The impedance data for the OER were analyzed using the equivalent circuit depicted in Figure 3b, which was adapted from the model reported by Negahdar et al.[14]. The circuit consists of a solution resistance (Rs) in series with a parallel combination of the charge-transfer resistance (R_{ct}) and a constant phase element (CPE), followed by a parallel Cp Rp branch. Here, Rs represents the electrolyte resistance, Rct corresponds to the interfacial charge-transfer resistance during oxygen evolution, CPE accounts for non-ideal capacitive behavior arising from surface heterogeneity, and the Cp‖Rp branch describes interfacial relaxation processes at lower frequencies. This model has been widely applied to describe the impedance response of alkaline OER systems. The EIS data obtained for the HMFOR (Figure 3c) exhibited incomplete and depressed semicircles, likely due to the contributions of double-layer charging, mass transfer, and diffusion. Therefore, the data were fitted using the equivalent circuit shown in Figure 3d, consisting of the solution resistance (R_u), a parallel combination of R_{ct} and a double-layer constant phase element (CPE_{Cdl}), followed by a diffusion-related constant phase element (CPE_{Diff}). A single CPE exponent (α) between 0.5 and 0.62 was used for both CPE_{Cdl} and CPE_{Diff} to account for diffusion-related non-ideal behavior[15]. In this model, R_{ct} represents the charge-transfer resistance associated with HMF oxidation, CPE_{Cdl} corresponds to the non-ideal double-layer capacitance, and CPE_{Diff} accounts for diffusion-controlled behavior and mass-transport effects that become significant during the HMFOR at higher current densities.

3.2.2. EIS data analysis. The EIS results provide a quantitative assessment of the interfacial Rct associated with the OER and HMFOR of the prepared catalysts. As shown in Figure 3a,c and summarized in Table S3, all samples exhibit substantially lower Rct values during the HMFOR than during the OER, confirming that HMF oxidation is kinetically more favorable under the investigated conditions. Among the stepwise-deposited catalysts, the Co-first sample exhibited an Rct of 0.0485 Ω during the HMFOR, significantly lower than its corresponding OER value (0.272 Ω). A similar trend was observed for the Ni-first sample, where the HMFOR and OER Rct values were 0.0490 and 0.270 Ω, respectively. These results indicate that the presence of HMF facilitates interfacial charge transfer by reducing the kinetic barrier associated with the anodic process. The mixed sample exhibited relatively higher Rct values for both reactions, with an HMFOR Rct of 0.0541 Ω, which, although lower than its OER value, remained higher than those of the other catalysts. This indicates that, despite the more favorable HMFOR kinetics, interfacial charge transfer was less efficient for the mixed sample, consistent with the lower anodic activity observed in the LSV results. In contrast, the pulse-deposited sample exhibited the lowest HMFOR Rct (0.0392 Ω), indicating enhanced

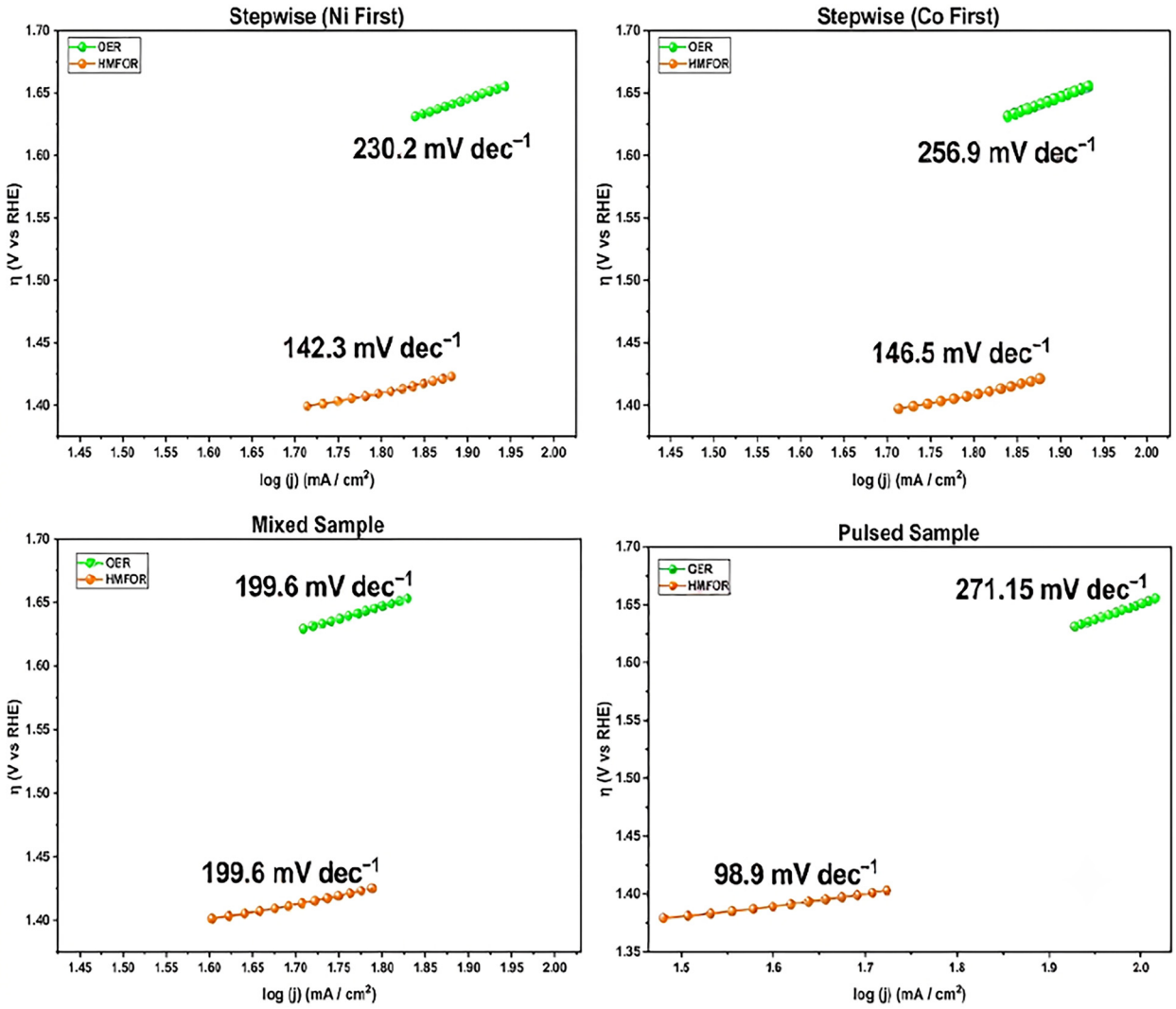

Figure 2. Tafel plots for the OER and the HMFOR performed over the prepared Ni–Co catalysts in 1.0 M KOH with the addition of 10.0 mM HMF

interfacial electron-transfer kinetics. This observation agrees with its superior HMFOR performance in the LSV and Tafel analyses, confirming that pulse deposition promotes faster HMFOR kinetics and more efficient charge-transfer behavior.

The C_{dl} values obtained from linear fitting of the current density versus scan rate plot (Figure S7) reflect clear differences in the electrochemically accessible surface areas among the samples. Specifically, the mixed and stepwise (Co-first) samples (Figures S7b,c) exhibit the highest C_{dl} values of 9.44 and 9.67 mF cm^{-2}, respectively. These results indicate that these catalysts contain more abundant electrochemically accessible active sites. In contrast, the Ni-first catalyst exhibited the lowest C_{dl} value, consistent with reduced surface exposure. However, the observed ECSA trend (Table S4) did not directly correlate with catalytic performance during the HMFOR. Specifically, the mixed sample exhibited a relatively higher Tafel slope for the HMFOR, together with the highest charge-transfer resistance (0.0541 Ω), reflecting less favorable HMFOR kinetics. Similar behavior was observed for the Co-first catalyst, wherein its high C_{dl} did not translate into enhanced activity. In contrast, the pulse-deposited catalyst demonstrated the most favorable HMFOR performance, as evidenced by its low Tafel slope and R_{ct}. Similar behavior has been reported in previous studies, where the catalytic performance was found to depend not only on the number of active sites, but also on their intrinsic activity and accessibility [16,17].

To analyze the reaction products, chronoamperometric electrolysis was conducted separately at 1.50 V vs. RHE, and the resulting HMF conversion and FDCA yield were quantified using HPLC. To evaluate the catalytic efficiency for HMF oxidation, the HMF conversion was calculated using Equation (S2), while the FDCA yield was calculated using Equation (S3). As shown in Figure S9, the HMF conversion reached 100% after 60 min and remained constant during the electrolysis period, indicating the rapid consumption of HMF on the pulse-deposited Ni–Co catalyst. However, although the FDCA yield gradually increased over time, it reached only 28.52% after 180 min. This notable difference between HMF conversion and FDCA yield suggests that although HMF was consumed, it was not fully converted into FDCA. This implies the formation and accumulation of intermediate products, such as HMFCA, which were not completely

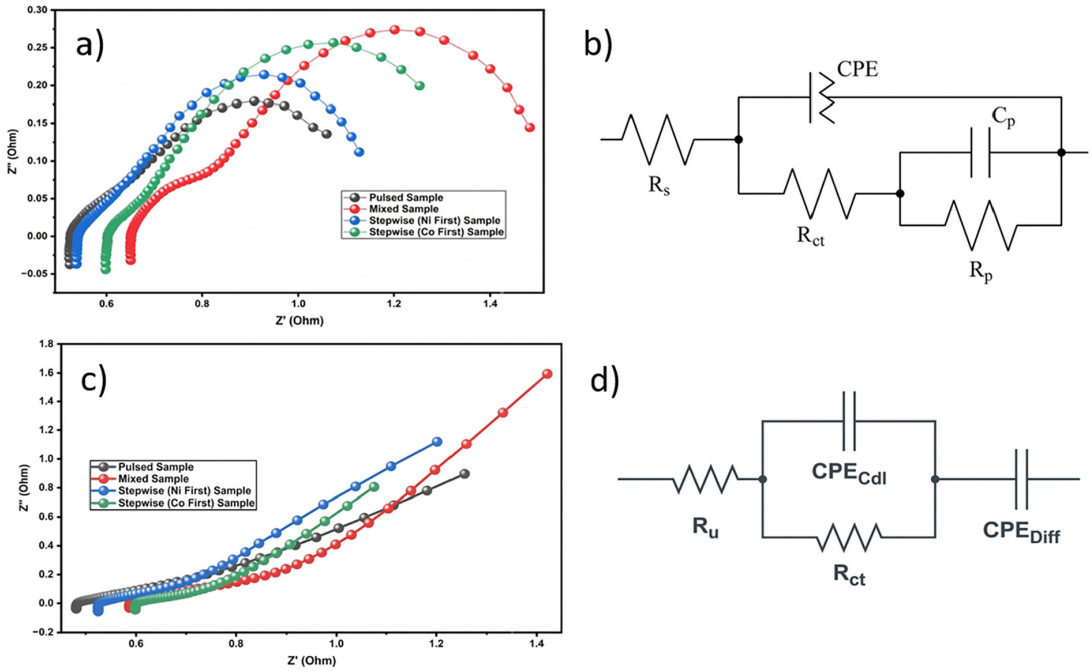

Figure 3. EIS Nyquist plots and corresponding equivalent circuit models for (a,b) the OER and (c,d) the HMFOR on the prepared samples. The equivalent circuit in (b) was adapted from the model reported by Negahdar et al.[14]

oxidized to FDCA under the applied conditions. Additionally, the gradual increase in FDCA yield suggests that the later oxidation steps were slower than the initial HMF oxidation process. Since electrolysis was performed at a single applied potential, further optimization of the reaction conditions may therefore be required.

4. CONCLUSIONS

In this study, Ni–Co bimetallic catalysts were successfully fabricated on NF via different electrodeposition strategies, including stepwise, mixed, and pulsed deposition. It was revealed that the deposition approach plays a crucial role in tailoring the catalyst surface structure and electrochemical performance. Among the investigated catalysts, the pulse-deposited catalyst exhibited the most favorable performance for HMF oxidation, which can be attributed to its optimized surface architecture that promotes mass transport and more efficient charge-transfer behavior. Electrochemical analysis revealed that the pulse-deposited sample achieved the lowest Tafel slope (98.9 mV dec^{-1}) and the smallest charge-transfer resistance (0.0392 Ω), indicating enhanced HMFOR kinetics. Although some catalysts exhibited higher electrochemically active surface areas, this did not directly translate into superior HMFOR performance, highlighting the importance of the intrinsic activity and active site accessibility. HPLC confirmed complete HMF conversion during electrolysis, although the FDCA yield reached only 28.52% after 180 min at 1.50 V vs. RHE. These findings imply the formation of intermediate products during the oxidation pathway. Thus, future work will focus on optimizing the applied potential and electrolysis conditions to enhance FDCA selectivity and promote the complete oxidation of intermediate products. In addition, detailed product analysis will be performed to better understand the reaction pathway and improve the overall efficiency of the HMFOR process.

AFFILIATIONS AND AUTHOR DETAILS

Undergraduate Author

Joud Aljohani – *Department of Chemical Engineering, King Fahd University of Petroleum & Minerals, Dhahran 31261, Saudi Arabia;* 0009-0003-7280-3697
Email: s202281540@kfupm.edu.sa

Corresponding Author

Wasif Farooq – *Research Mentor, Associate Professor, Department of Chemical Engineering, King Fahd University of Petroleum & Minerals, Dhahran 31261, Saudi Arabia;* 0000-0002-4882-0097
Email: wasif@kfupm.edu.sa

ACKNOWLEDGEMENTS

The authors acknowledge the Department of Chemical Engineering and the Interdisciplinary Research Center at King Fahd University of Petroleum and Minerals for their support. They also thank Dr. Akilarasan Muthumariappan, Dr. Muhammad Tahir, and the technical staff for their valuable guidance and assistance with specimen preparation and testing.

REFERENCES

(1) Ojelabi, O., Thiensuwan, N., Chotirattanachote, A., Kaewngam, C., Rashid, U., and Ngamcharussrivichai, C. (2026). Toward sustainable production of 5-hydroxymethylfurfural from biomass-derived glucose through acidity-tuned zeolite catalysts. Sustain. Chem. Pharm. *51*. https://doi.org/10.1016/j.scp.2026.102405.

(2) Van Putten, R.J., Van Der Waal, J.C., De Jong, E., Rasrendra, C.B., Heeres, H.J., and De Vries, J.G. (2013). Hydroxymethylfurfural, a versatile platform chemical made from renewable resources. *Chem. Rev.* **113**(3), 1499–1597. https://doi.org/10.1021/cr300182k.

(3) Lotfi, N., and Barati Darband, G. (2024). A review on electrodeposited metallic Ni-based alloy nanostructure for electrochemical hydrogen evolution reaction. *International Journal of Hydrogen Energy*, 70, 301–314. https://doi.org/10.1016/j.ijhydene.2024.05.121.

(4) Zhang, S., Yang, X., Ma, L., Ma, J., and Gao, H. (2025). Efficient electrocatalytic oxidation of 5-hydroxymethylfurfural to 2,5-furandicarboxylic acid using an amorphous bimetallic Ni–Co hydroxide with filamentous structure in alkaline media. Mater. Today Chem. *49*, 103095. https://doi.org/10.1016/j.mtchem.2025.103095.

(5) Chen, Z., Zhang, G., Jiang, J., Feng, X., Li, W., Xiang, X., and Linling, G. (2024). The progress of research on vacancies in HMF electrooxidation. *Front. Chem.* 12, 1416329. https://doi.org/10.3389/fchem.2024.1416329.

(6) Garduño-Ibarra, I.R., Yan, Z., Ebrahim, S.A., Baranova, E., González-Cobos, J., Prévot, M., and Vernoux, P. (2025). Ni-Based Catalysts for 5-Hydroxymethylfurfural Electrooxidation Coupled with Hydrogen Production. *ChemElectroChem* 12(13), e202500067. https://doi.org/10.1002/celc.202500067.

(7) Li, W., Yin, D., Liu, W., Li, Y., and Wu, Y. (2025). NiCo(OH)2/NiCo2O4 as a Heterogeneous Catalyst for the Electrooxidation of 5-Hydroxymethylfurfural. Inorganics (Basel). *13*. https://doi.org/10.3390/inorganics13070211.

(8) Liu, F.B., Lin, N., Cong, L.C., Li, X.X., Han, F.Y., Xin, D.Y., and Lin, H.B. (2023). Industrially Promising β-Ni(OH)2 Nanosheets Self-Supported Electrode for Highly Efficient Electrooxidation of 5-Hydroxymethylfurfural. ChemCatChem *15*. https://doi.org/10.1002/cctc.202300765.

(9) Goldstein, J.I., Newbury, D.E., Michael, J.R., Ritchie, N.W.M., Henry, J., Scott, J., and Joy, D.C. Scanning Electron Microscopy and X-Ray Microanalysis.

(10) Lu, L., Wen, C., Wang, H., Li, Y., Wu, J., and Wang, C. (2023). Tailoring the electron structure and substrate adsorption energy of Ni hydroxide via Co doping to enhance the electrooxidation of biomass-derived chemicals. J. Catal. *424*, 1–8. https://doi.org/10.1016/j.jcat.2023.05.001.

(11) Tchekwagep, P.M.S., Banks, C.E., Crapnell, R.D., Farsak, M., and Kardaş, G. (2025). Electrochemical synthesis of NiCo layered double hydroxides on nickel-coated graphite for water splitting: Understanding the electrochemical experimental parameters. RSC Adv. *15*, 3969–3978. https://doi.org/10.1039/d4ra08053j.

(12) Zhang, D., Tang, X., Yang, Z., Yang, Y., and Li, H. (2022). Construction of honeycomb-like Te-doped NiCo-LDHs for aqueous supercapacitors and as oxygen evolution reaction electrocatalysts. Mater. Adv. *3*, 1286–1294. https://doi.org/10.1039/d1ma00688f.

(13) Bard, A.J., Faulkner, L.R., and Wiley, J. (1983). Electrochemical Methods, Fundamentals and Applications.

(14) Negahdar, L., Zeng, F., Palkovits, S., Broicher, C., and Palkovits, R. (2019). Mechanistic Aspects of the Electrocatalytic Oxygen Evolution Reaction over Ni−Co Oxides. ChemElectroChem *6*, 5588–5595. https://doi.org/10.1002/celc.201901265.

(15) Lazanas, A.C., and Prodromidis, M.I. (2023). Electrochemical Impedance Spectroscopy-A Tutorial. *ACS Meas. Sci. Au* **3**(3), 162–193. https://doi.org/10.1021/acsmeasuresciau.2c00070.

(16) Lei, J., Zhang, H., Yang, J., Ran, J., Ning, J., Wang, H., and Hu, Y. (2025). Structural designs and mechanism insights into electrocatalytic oxidation of 5-hydroxymethylfurfural. *J. Energy Chem.* 100, 443–462. https://doi.org/10.1016/j.jechem.2024.08.066.

(17) Molinaro, J.M., Swartzentruber, J., Ledger, V.W., Fredericks, Z.T., Alonso, D.M., and Wettstein, S.G. (2025). Recent developments in solvent and catalyst selection for 5-hydroxymethylfurfural oxidation to 2,5-furandicarboxylic acid. *Energy Adv.* **4**, 1213–1243. https://doi.org/10.1039/d5ey00028a.